Journal of Pharmaceutical Analysis 15 (2025) 101107

Contents lists available at ScienceDirect

Journal of Pharmaceutical Analysis

journal homepage: www.elsevier.com/locate/jpa

Short communication

Radiosynthesis and preclinical evaluation of [^{18}F]AlF-labeled HBED-CC-FAPI derivatives for imaging of cancer-associated fibroblasts

Haiyan Hong [a, b], Yan Zhang [c], Jinping Qiao [d], Wensheng Zhang [b, ***], Lin Zhu [d, **], Jiehua Xu [a, *]

[a] Department of Nuclear Medicine, Zhuhai People's Hospital (Zhuhai Clinical Medical College of Jinan University), Zhuhai, Guangdong, 519000, China
[b] Engineering Research Center of Natural Medicine, Ministry of Education, Beijing Normal University at Zhuhai, Zhuhai, Guangdong, 519087, China
[c] Department of Nuclear Medicine, Beijing Tsinghua Changgung Hospital (School of Clinical Medicine, Tsinghua University), Beijing, 102218, China
[d] Key Laboratory of Radiopharmaceuticals, Ministry of Education, Beijing Normal University, Beijing, 100875, China

ARTICLE INFO

Article history:
Received 6 July 2024
Received in revised form
10 September 2024
Accepted 18 September 2024
Available online 21 September 2024

Fibroblast activation protein (FAP) is overexpressed in cancer-associated fibroblasts across various cancer types. Numerous radiolabeled FAP inhibitors (FAPIs) (Fig. S1A) currently under clinical investigation have shown remarkable potential in cancer theranostics. Our previous work [1] introduced the [^{68}Ga]Ga-*N*,*N*′-bis[2-hydroxy-5-(carboxyethyl)benzyl]ethylenediamine-*N*,*N*′-diacetic acid (HBED-CC)-FAPI derivatives ([^{68}Ga]Ga-**4**, [^{68}Ga]Ga-**5**, [^{68}Ga]Ga-**6**, and [^{68}Ga]Ga-**7**) (Fig. S1B), which incorporate an *N*-(4-quinolinoyl)-Gly-(2-cyanopyrrolidine) FAP-binding scaffold. These derivatives demonstrated superior tumor uptake and retention compared to the commonly used [^{68}Ga]Ga-1,4,7,10-tetraazacyclododecane-1,4,7,10-tetraacetic acid (DOTA)-FAPI-04 [1] (Fig. S1A). The HBED-CC chelator, initially used for ^{68}Ga labeling, has been adapted for ^{18}F labeling through [^{18}F]AlF chelation [2–5] (Fig. S1C). Due to the highly desirable physical characteristics of ^{18}F, such as its half-life ($t_{1/2}$) of 110 min, 97% β^+ decay, and a positron energy ($E_{\beta+}$) of 630 keV, making it ideal for nuclear medicine applications. In this study, the [^{68}Ga]Ga-HBED-CC-FAPI derivatives were successfully converted to [^{18}F]AlF-HBED-CC-FAPIs through [^{18}F]AlF chelation. The radiofluorination of HBED-CC-FAPI derivatives (**4**, **5**, **6**, and **7**) to form [^{18}F]AlF-HBED-CC conjugates was achieved with success (Fig. S1B). The stability and biological properties, including FAP-targeting and *in vivo* tumor uptake, of these ^{18}F agents were evaluated and compared with the corresponding [^{68}Ga]Ga-FAPI imaging agent, [^{68}Ga]Ga-**6** [1], previously optimized for FAP-positive tumor imaging.

The materials and methods used for [^{18}F]AlF labeling and bioevaluation are detailed in the Supplementary data. For [^{18}F]AlF labeling, purified [^{18}F]fluoride solution was combined with derivatives **4**, **5**, **6**, or **7** (HBED-CC-FAPIs) to form [^{18}F]AlF-HBED-CC-FAPIs according to a method reported previously [2]. Favorable and consistent radiolabeling efficiency (69%–80%) was obtained, and radiochemical yields and radiochemical purities were > 55% and > 95%, respectively (Table 1 and Fig. S2). Chemical identifications of [^{18}F]AlF-HBED-CC-FAPIs were performed, and the results are consistent with the corresponding "cold" [^{19}F]AlF-HBED-CC-FAPIs (Figs. S3–S7).

The [^{18}F]AlF-HBED-CC-FAPIs were consistently stable for at least 2 h in ethanol or saline with > 90% radiochemical purities (Fig. 1A). Moderate *in vivo* plasma stabilities of [^{18}F]AlF-HBED-CC-FAPIs in mice are shown in Table S1, which are similar to those of the [^{18}F]AlF-prostate-specific membrane antigen (PSMA)-11 and [^{18}F]AlF-P16-093 [2,3]. Notably, [^{18}F]AlF-HBED-CC-FAPIs, [^{18}F]AlF-PSMA-11, and [^{18}F]AlF-P16-093 employ the same chelate portion, [^{18}F]AlF-HBED-CC. A previous study evaluated the blood stability and defluorination of [^{18}F]AlF-PSMA-11 in patients, and the results showed no significant *in vivo* metabolism [5]. Therefore, the *in vivo* stabilities of these [^{18}F]AlF-HBED-CC agents in humans might be very similar.

[^{18}F]AlF-HBED-CC-FAPIs were incubated with FAP-positive HT1080-hFAP cells and FAP-negative HT1080 cells at 37 °C for 2 h to evaluate the FAP binding specificities and affinities. [^{68}Ga]Ga-**6** was used as a positive control. As shown in Fig. 1B and Table S2, [^{18}F]AlF-HBED-CC-FAPIs ([^{18}F]AlF-**4**, [^{18}F]AlF-**5**, [^{18}F]AlF-**6**, and [^{18}F]AlF-**7**) exhibited rapid cellular uptake and internalization at the initial time point (15 min), which increased and reached a stable level over time. The dimeric radiotracers ([^{18}F]AlF-**6** and [^{18}F]AlF-**7**)

* Corresponding author.
** Corresponding author.
*** Corresponding author.
E-mail addresses: zws@bnu.edu.cn (W. Zhang), zhulin@bnu.edu.cn (L. Zhu), xujhgz3@163.com (J. Xu).
Peer review under responsibility of Xi'an Jiaotong University.

https://doi.org/10.1016/j.jpha.2024.101107

Table 1
Radiosynthesis results of [^{18}F]AlF-*N*,*N*′-bis[2-hydroxy-5-(carboxyethyl)benzyl]ethylenediamine-*N*,*N*′-diacetic acid (HBED-CC)-fibroblast activation protein (FAP) inhibitors (FAPIs). Data are presented as mean ± standard deviation (SD) ($n = 10$).

Radiotracer	Labeling efficiency (%)[a]		Radiochemical yield (%)[b]	Radiochemical purity (%)		Retention factor	Retention time (min)[c]	Radioactivity (MBq)[d]	Molar activity (10^{15} Bq/mol)[e]
	TLC	HPLC		TLC	HPLC	TLC	HPLC		
[^{18}F]AlF-**4**	73.8 ± 3.9	77.8 ± 4.6	61.9 ± 4.6	95.9 ± 0.3	97.0 ± 0.9	0.5–0.6	9.8	370–555	9.3–13.9
[^{18}F]AlF-**5**	69.7 ± 1.6	76.1 ± 3.3	56.9 ± 2.6	95.8 ± 0.7	97.4 ± 1.4	0.7–0.8	9.7		
[^{18}F]AlF-**6**	76.0 ± 4.1	80.4 ± 3.9	65.6 ± 5.5	96.3 ± 0.6	99.5 ± 0.4	0.3–0.4	9.3		
[^{18}F]AlF-**7**	70.8 ± 3.1	75.0 ± 1.7	63.0 ± 2.2	96.5 ± 0.5	99.0 ± 0.7	0.4–0.5	9.4		

[a] Labeling efficiency was determined by radio-thin layer chromatography (TLC) and radio-high performance liquid chromatography (HPLC) analysis of crude product.
[b] Radiochemical yield was calculated as ((radioactivity of purified product/initially added radioactivity) × 100%) and was decay-corrected.
[c] Retention time was obtained from representative radio-HPLC profile (Fig. S2).
[d] Radioactivity of purified product.
[e] Molar activity was calculated as (radioactivity of purified product ÷ initially-added amount of ligand (40 nmol)).

showed higher total and internalized absorption than the corresponding monomer radiotracers ([^{18}F]AlF-**4** and [^{18}F]AlF-**5**), which was in accordance with [^{68}Ga]Ga-HBED-CC-FAPIs reported previously [1]. Cellular uptakes of [^{18}F]AlF-HBED-CC-FAPIs in FAP-positive HT1080-hFAP cells were significantly blocked with a blocking efficiency of > 90% (Fig. 1C and Table S2) in the presence of 3 μM DOTA-FAPI-04 (a known FAPI). Moreover, [^{18}F]AlF-HBED-CC-FAPIs showed negligible uptake in FAP-negative HT1080 cells (Fig. 1C and Table S2). The results demonstrated that [^{18}F]AlF-HBED-CC-FAPIs and the known FAPI, DOTA-FAPI-04, are competing for the same FAP binding sites, and the cellular bindings of [^{18}F]AlF-HBED-CC-FAPIs are due to specific binding to FAP. The results of cell binding studies were similar to those reported for [^{68}Ga]Ga-HBED-CC-FAPIs [1].

Mice-bearing U87MG tumors (FAP+) were used to perform *in vivo* static positron emission tomography/computed tomography (PET/CT) imaging. Maximum intensity projection (MIP) images were obtained at 30, 60, 120, and 180 min post-injection (Fig. 1D). All of the [^{18}F]AlF-HBED-CC-FAPIs ([^{18}F]AlF-**4**, [^{18}F]AlF-**5**, [^{18}F]AlF-**6**, and [^{18}F]AlF-**7**) quickly accumulated in the tumor at 30 min post-injection and excreted mainly through the hepatobiliary system. Although [^{18}F]AlF-**5** and [^{18}F]AlF-**7** showed rapid and clear tumor accumulation, high uptake and slow washout from the gallbladder, intestine ([^{18}F]AlF-**5**), and liver ([^{18}F]AlF-**7**) made both radiotracers unacceptable as FAP-targeted agents. In addition, [^{18}F]AlF-**4** was highly concentrated in the tumor and intestine and showed a higher tumor uptake than [^{18}F]AlF-**5** and [^{18}F]AlF-**7**. However, [^{18}F]AlF-**4** exhibited a faster tumor washout at 120 min post-injection. Among this series of [^{18}F]AlF-HBED-CC-FAPIs ([^{18}F]AlF-**4**, [^{18}F]AlF-**5**, [^{18}F]AlF-**6**, and [^{18}F]AlF-**7**), the tumor uptake, retention, and background clearance of [^{18}F]AlF-**6** was the most optimal and superior to that of the corresponding [^{68}Ga]Ga-**6**.

Two of the most promising agents, [^{18}F]AlF-**4** and [^{18}F]AlF-**6**, were further evaluated via a biodistribution study (dissection and sample counting) using the U87MG tumor-bearing mice model, and the results were compared with those of [^{68}Ga]Ga-**6** under the same conditions. Biodistribution data (Fig. 1E and Tables S3–S6) showed similar *in vivo* pharmacokinetics for [^{18}F]AlF-**4**, [^{18}F]AlF-**6**, and [^{68}Ga]Ga-**6** as that measured via PET/CT imaging. Three radiolabeled FAPIs displayed excellent tumor uptake with values of 17.51 ± 1.49, 41.16 ± 1.52, and 34.32 ± 0.95 %ID/g for [^{18}F]AlF-**4**, [^{18}F]AlF-**6**, and [^{68}Ga]Ga-**6** at 60 min post-injection, respectively. Among these, [^{18}F]AlF-**6** showed the highest tumor uptake (41.16 ± 1.52 %ID/g). When a known FAP-targeted agent (DOTA-FAPI-04) was co-injected for a blocking study, tumor uptakes were considerably reduced (0.47 ± 0.15, 4.18 ± 0.30, and 3.05 ± 0.61 %ID/g, 60 min), indicating that [^{18}F]AlF-**4**, [^{18}F]AlF-**6**, and [^{68}Ga]Ga-**6** were competing to FAP binding sites of U87MG tumors in mice. Their binding to the FAP was specific and reversible. At all measured time points, [^{18}F]AlF-**6** exhibited better tumor uptake and retention than [^{18}F]AlF-**4** (60 min: 41.16 ± 1.52 vs. 17.51 ± 1.49 %ID/g, 120 min: 40.33 ± 4.12 vs. 12.77 ± 0.82 %ID/g, respectively). [^{18}F]AlF-**6** showed higher tumor-to-organ ratios than [^{18}F]AlF-**4** (Table S6). Compared to [^{68}Ga]Ga-**6**, [^{18}F]AlF-**6** revealed improved tumor uptake (60 min: 34.32 ± 0.95 vs. 41.16 ± 1.52 %ID/g, 120 min: 33.07 ± 4.90 vs. 40.33 ± 4.12 %ID/g) (Fig. 1F), which was also superior to that of the widely used [^{68}Ga]Ga-DOTA-FAPI-04 [1]. [^{18}F]AlF-**6** showed similar tumor-to-organ ratios to [^{68}Ga]Ga-**6** (Table S6). Bone uptake of [^{18}F]AlF-**6** was slightly higher. Similar results were also observed and reported previously for [^{18}F]AlF-HBED-CC-based PSMA-targeting conjugates in preclinical studies [2,3]. However, minor bone uptake showed negligible impact on diagnostic imaging for cancer patients [4,5]. A more detailed discussion regarding bone uptake is shown in the Supplementary data.

The favorable physical and biological properties of [^{18}F]AlF-**6** will offer several advantages over [^{68}Ga]Ga-**6** as a PET imaging agent: 1) it exhibits excellent selective binding and higher *in vivo* tumor uptake; 2) its longer half-life is favorable for acquiring delayed images with high contrast; 3) it enables long-distance delivery of ^{18}F-labeled tracers; 4) its higher positron yield and lower positron energy improve the resolution of PET images, which benefit the detection of small lesions; and 5) a higher activity level of ^{18}F generated by cyclotron allows multiple doses of the product in one radiosynthesis, which is sufficient for a larger number of patients. Further studies of [^{18}F]AlF-**6** in clinical settings are warranted to validate its usefulness for FAP-targeted cancer detection.

In summary, [^{18}F]AlF-HBED-CC-FAPI derivatives ([^{18}F]AlF-**4**, [^{18}F]AlF-**5**, [^{18}F]AlF-**6**, and [^{18}F]AlF-**7**) were successfully prepared via an easy and efficient one-pot fluorination reaction. [^{18}F]AlF-**6** exhibited specific tumor uptake and retention in a mice-tumor model. The results suggest that [^{18}F]AlF-**6** is a promising ^{18}F-labeled FAP-targeting agent suitable for widespread clinical application.

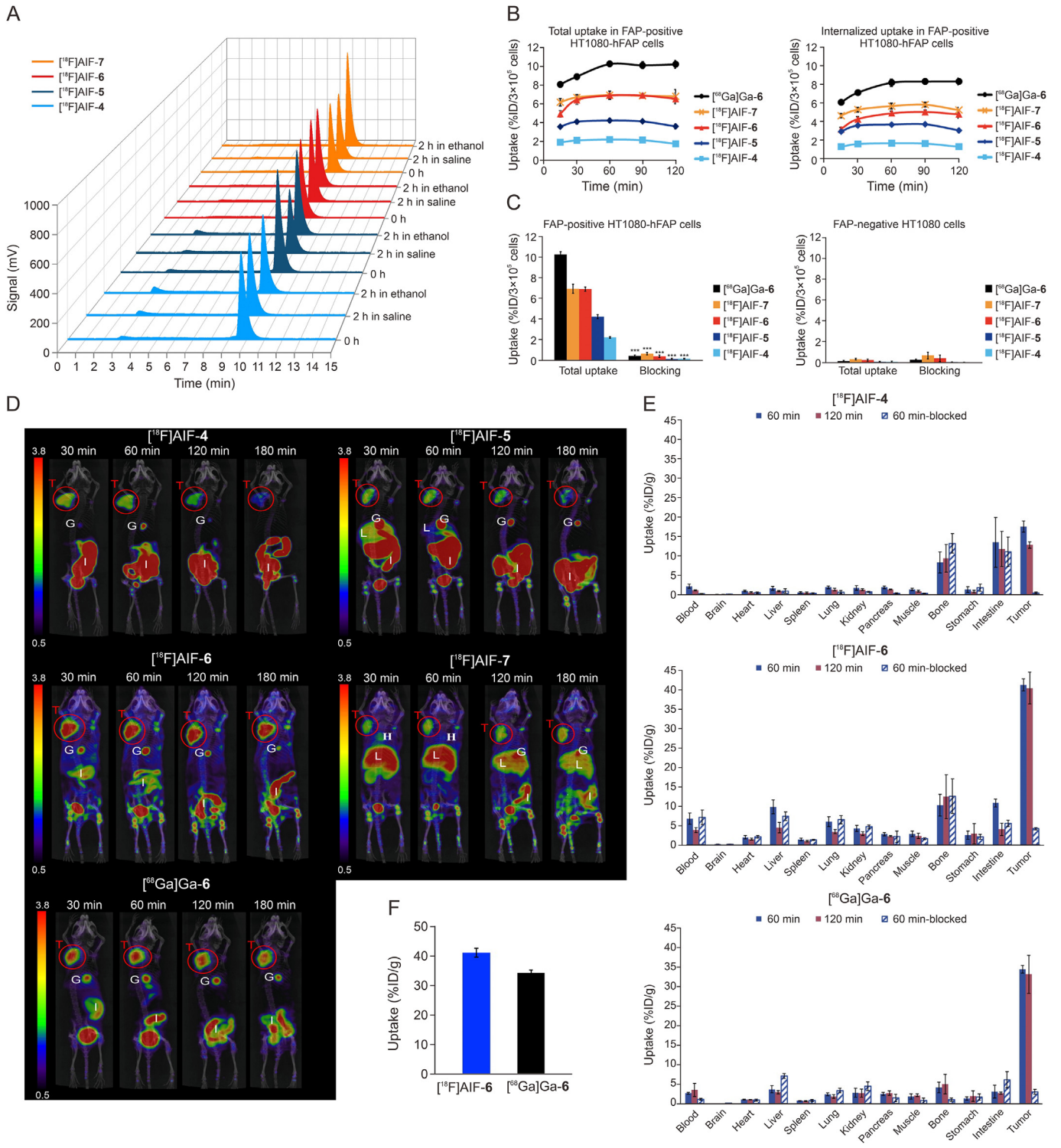

Fig. 1. *In vitro* stability and biological properties (fibroblast activation protein (FAP)-targeting properties and *in vivo* tumor uptake) of [^{18}F]AlF-*N*,*N*′-bis[2-hydroxy-5-(carboxyethyl) benzyl]ethylenediamine-*N*,*N*′-diacetic acid (HBED-CC)-FAP inhibitors (FAPIs) ([^{18}F]AlF-**4**, [^{18}F]AlF-**5**, [^{18}F]AlF-**6**, and [^{18}F]AlF-**7**). (A) Representative radio-high performance liquid chromatography (HPLC) profiles of *in vitro* stabilities of [^{18}F]AlF-HBED-CC-FAPIs after incubating in saline or ethanol at 37 °C for 2 h (n = 3/time points). (B) Total and internalized uptake of [^{18}F]AlF-**4**, [^{18}F]AlF-**5**, [^{18}F]AlF-**6**, [^{18}F]AlF-**7**, and [^{68}Ga]Ga-**6** in FAP-positive HT1080-hFAP cells at 37 °C for 15, 30, 60, 90, and 120 min, respectively. Data are presented as the mean ± standard deviation (SD) (n = 3). (C) Blocking studies (incubated with 3 μM 1,4,7,10-tetraazacyclododecane-1,4,7,10-tetraacetic acid (DOTA)-FAPI-04 for 60 min) of [^{18}F] AlF-HBED-CC-FAPIs and [^{68}Ga]Ga-**6** in FAP-positive HT1080-hFAP cells and FAP-negative HT1080 cells. Data are presented as the mean ± SD (n = 3). $^{***}P < 0.001$. (D) Representative static coronal positron emission tomography/computed tomography (PET/CT) images of [^{18}F]AlF-**4**, [^{18}F]AlF-**5**, [^{18}F]AlF-**6**, [^{18}F]AlF-**7**, and [^{68}Ga]Ga-**6** in mice bearing U87MG tumors (FAP+). Red circles indicate the tumor lesions (T: U87MG tumor, G: gallbladder, L: liver, and H: heart). (E) Biodistribution of [^{18}F]AlF-**4**, [^{18}F]AlF-**6**, and [^{68}Ga]Ga-**6** in U87MG tumor-bearing mice. Blocking studies were co-injected with DOTA-FAPI-04 (40 nmol/mouse). Data are presented as the mean ± SD (n = 4). (F) Tumor uptake of [^{18}F]AlF-**6** and [^{68}Ga]Ga-**6** in U87MG tumor-bearing mice at 1 h post-injection. Data are presented as the mean ± SD (n = 4).

Ethical statement

All animal studies followed the National Institutes of Health (NIH), USA Guidelines for the Care and Use of Laboratory Animals, and were approved by the Laboratory Animal Ethics Committee of Jinan University (Approval No.: 20210306-010).

CRediT authorship contribution statement

Haiyan Hong: Conceptualization, Data curation, Formal analysis, Investigation, Methodology, Project administration, Validation, Visualization, Writing - original draft, Writing - reviewing & editing; **Yan Zhang:** Formal analysis, Project administration, Visualization, Writing - reviewing & editing; **Jinping Qiao:** Data curation, Formal analysis, Resources, Writing - reviewing & editing; **Wensheng Zhang:** Supervision, Writing - reviewing & editing; **Lin Zhu** and **Jiehua Xu:** Conceptualization, Funding acquisition, Project administration, Resources, Supervision, Writing - reviewing & editing.

Declaration of competing interest

The authors declare that there are no conflicts of interest.

Acknowledgments

This study was supported by the grants provided by Zhuhai People's Hospital, China (Grant No.: 2021KYQD-03) and the National Natural Science Foundation of China (Grant No.: 22176016). The authors thank Prof. Hank F. Kung (Department of Radiology, University of Pennsylvania, Philadelphia, PA, USA) for the assistance in study design and manuscript preparation, Prof. Zuoxiang He (Department of Nuclear Medicine, Beijing Tsinghua Changgung Hospital (School of Clinical Medicine, Tsinghua University), Beijing, China) for the assistance in providing [^{18}F]fluoride, and Dr. Shisong Han (Department of Nuclear Medicine, Zhuhai People's Hospital (Zhuhai Clinical Medical College of Jinan University), Zhuhai, China) for the suggestions in study execution. We thank LetPub (www.letpub.com.cn) for its linguistic assistance during the preparation of this manuscript.

Appendix A. Supplementary data

Supplementary data to this article can be found online at https://doi.org/10.1016/j.jpha.2024.101107.

References

[1] H. Hong, Z. Zha, R. Zhao, et al., [^{68}Ga]Ga-HBED-CC-FAPI derivatives with improved radiolabeling and specific tumor uptake, Mol. Pharm. 20 (2023) 2159–2169.
[2] Z. Zha, S.R. Choi, K. Ploessl, et al., Radiolabeling optimization and preclinical evaluation of the new PSMA imaging agent [^{18}F]AlF-P16-093, Bioconjug. Chem. 32 (2021) 1017–1026.
[3] S. Lütje, G.M. Franssen, K. Herrmann, et al., *In vitro* and *in vivo* characterization of an ^{18}F-AlF-labeled PSMA ligand for imaging of PSMA-expressing xenografts, J. Nucl. Med. 60 (2019) 1017–1022.
[4] R. Zhao, M. Ke, J. Lv, et al., First-in-human study of PSMA-targeting agent, [^{18}F]AlF-P16-093: Dosimetry and initial evaluation in prostate cancer patients, Eur. J. Nucl. Med. Mol. Imaging 51 (2024) 1753–1762.
[5] S. Piron, K. De Man, N. Van Laeken, et al., Radiation dosimetry and biodistribution of ^{18}F-PSMA-11 for PET imaging of prostate cancer, J. Nucl. Med. 60 (2019) 1736–1742.